LiCo$_x$Mn$_{1-x}$PO$_4$/C: A High Performing Nanocomposite Cathode Material for Lithium Rechargeable Batteries

Chandrasekaran Nithya, Ramasamy Thirunakaran, Arumugam Sivashanmugam, and Sukumaran Gopukumar*[a]

Abstract: Pristine and Co-doped LiMnPO$_4$ have been synthesized by the sol-gel method using glycine as a chelating agent and the carbon composites were obtained by the wet ball mill method. The advantage of this method is that it does not require an inert atmosphere (economically viable) and fa- cilitates a shorter time for synthesis. The LiCo$_{0.09}$Mn$_{0.91}$PO$_4$/C nanocomposites exhibit the highest coulombic effi- ciency of 99%, delivering a capacity of approximately 160 mAhg^{-1} and retain a capacity of 96.3% over the investi- gated 50 cycles when cycled between 3–4.9 V at a charge/discharge rate of 0.1 C.

Keywords: cobalt · doping · inter- calations · lithium · sol-gel process- es

Introduction

Commercially used lithium-ion batteries possessing LiCoO$_2$ cathode materials have advantages such as, easy synthesis and excellent cyclability, however, they are toxic in nature and only deliver half of the theoretical capacity.[1] Recently, lithium iron phosphates (LiFePO$_4$) have attracted much in- terest owing to their lower toxicity, lower cost, better chemi- cal and thermal stabilities, and also the improved power ca- pability[2–9] when compared to the presently used LiCoO$_2$ cathode materials. LiFePO$_4$ materials exhibit stable olivine structures in which the three dimensional framework is sta- bilized by the strong covalent bonds between oxygen ions and the P^{5+}, thus resulting in PO$_4^{3-}$ tetrahedral polyanions.[2] Olivine transition metal phosphates do not undergo any structural deterioration during cycling owing to their struc- tural stability.

However, the low intrinsic electronic conductivity of LiFePO$_4$ material is a major problem.[9] The conductivity problem of LiFePO$_4$ has been solved by addition of conduc- tive additives, cation doping, nanoparticle synthesis, and sur- face modification.[10,11] LiCoPO$_4$ is another isomeric phos- phate-based cathode material, but this material has the drawback of significant capacity fading during cycling.[12] LiMnPO$_4$ is one of the most attractive cathode materials owing to the high redox potential of Mn^{2+}/Mn^{3+} versus Li/ Li$^+$ (4.1 V).[13] LiMnPO$_4$ possesses high theoretical specific capacity and high energy density, similar to LiFePO$_4$; how-

ever, it suffers many drawbacks that prevent the use of the Mn^{3+}/Mn^{2+} redox couple as a cathode material.[13] It exhib- its lower current durability, slower kinetics, and a smaller ef- fective energy density than LiFePO$_4$.[13] Delacourt and co- workers suggest that the reason for the poor electrochemical activity of LiMnPO$_4$ is a large kinetic barrier at the incom- patible interface of MnPO$_4$/LiMnPO$_4$.[14] Hydrothermal syn- thesis of electrochemically active LiMnPO$_4$ was reported by Liu and co-workers[15] and Fang and co-workers,[16] but ex- hibits poor capacity retention after only a few cycles.

To overcome the above problems of LiMnPO$_4$, there have been numerous approaches adopted by many research- ers.[17–25] Drezen and co-workers have reported that the re- duction of particle size of LiMnPO$_4$ in the range of 140– 220 nm resulted in the reversible capacity of 134 mAhg^{-1} at a charge rate of C/10.[17] Polyol-assisted synthesis of nano- sized LiMnPO$_4$ particles provides approximately 115 mAhg^{-1}.[18,19] Carbon coating is an effective method for improving the performance of LiMnPO$_4$ materials.[20–23] Off- stoichiometry LiMnPO$_4$ was investigated by Kang and co- workers,[24] and recently Martha and co-workers reported that Fe-doped LiMnPO4 cathode material retains 80% of the capacity in the flat region of 4.1 V versus Li/Li$^+$.[25] In all the previous reports, an inert atmosphere is used for the synthesis of LiMnPO$_4$ or its composites. In this work, we report for the first time the use of Co as the dopant in the Mn site and the corresponding carbon composites prepared under an atmosphere of air and its electrochemical perfor- mance between 3–4.9 V at different C-rates.

[a] C. Nithya, Dr. R. Thirunakaran, Dr. A. Sivashanmugam, Dr. S. Gopukumar
Electrochemical Power Systems Division
Central Electrochemical Research Institute
Karaikudi, Tamilnadu, 630 006 (India)
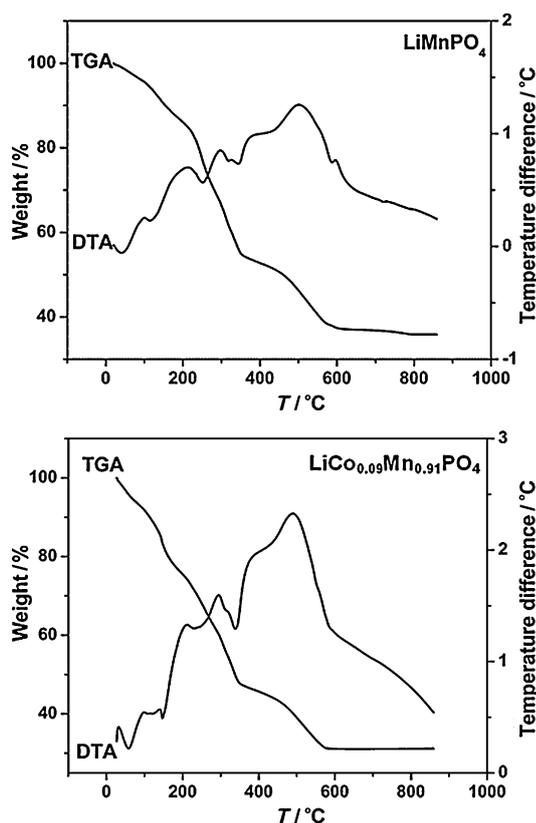Fax: (+91) 4565-227779
E-mail: deepika_41@rediffmail.com

Results and Discussion

Thermogravimetric (TG) and differential thermal analysis (DTA) curves of the LiMnPO$_4$ and Co-doped LiMnPO$_4$ ma- terials synthesized by the sol-gel method using glycine as a

Figure 1. TG/DTA curves of LiMnPO$_4$ and LiCo$_{0.09}$Mn$_{0.91}$PO$_4$ gel precursors synthesized by the sol-gel method.

Figure 2. XRD patterns of LiMnPO4/C and LiCo$_{0.09}$Mn$_{0.91}$PO$_4$/C.

chelating agent are shown in Figure 1. There are three weight loss zones in the TG curve of both the samples. The first weight loss zone (0–135 °C) corresponds to the loss of water molecules. Thermal decomposition above 135 °C leads to the evolution of ammonia and water of constitution begins to be liberated at 170 °C, and the maximum quantity of combined water is released in the second region (135–350 °C). Major weight loss occurs in the range 351–580 °C, attributed to the decomposition of acetate precursors. The corresponding exothermic peak centered at 500 °C is shown in the DTA curve, therefore, the temperature for synthesizing LiMnPO$_4$ and LiCo$_{0.09}$Mn$_{0.91}$PO$_4$ should be higher than 490 °C. However, a further increase in the temperature results in minimal change in the TG curve up to 850 °C. This may be attributed to the ordered olivine structure of LiMnPO$_4$ and LiCo$_{0.09}$Mn$_{0.91}$PO$_4$ becoming more complete within this temperature range.

Figure 2 shows the X-ray diffraction patterns of LiMnPO$_4$/C and LiCo$_{0.09}$Mn$_{0.91}$PO$_4$/C materials. All the materials showed a single phase with an ordered olivine structure indexed to the orthorhombic *Pnmb* space group free from impurities. This olivine structure may be described as a chain of edge sharing octahedra connected to one another by phosphate terahedra, MnPO$_4^-$, which are connected to one another by octahedrally coordinated lithium atoms.[26] After doping with Co, the intensity of the peaks slightly decreases, which indicates that the addition of dopant has a
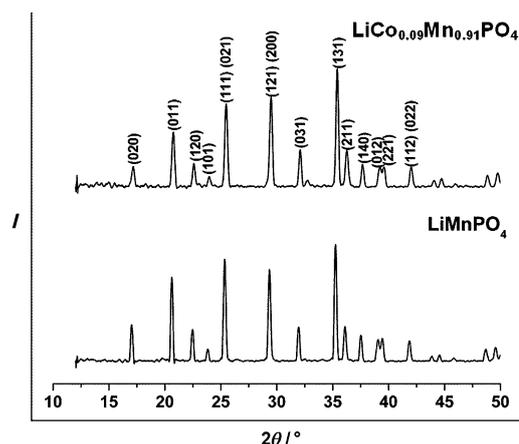
significant role in confining the growth of the particle size. The refined lattice parameters (*a*, *b*, *c* and cell volume) are (6.108, 10.513, 4.749, 304.95) and (6.129, 10.530, 4.769, 307.78) for LiMnPO$_4$/C and LiCo$_{0.09}$Mn$_{0.91}$PO$_4$/C composites, respectively, obtained by using the X′Pert High Score Plus software. According to Vegards's law,[27] substitution of Mn^{2+} (0.67 Å) at the 4C site by Co^{2+} (0.75 Å) cations causes an increase in the cell parameters and volume. As suggested by Ouyang and co-workers,[28] such an increase in the lattice parameters and cell volume will enhance the lithium-ion diffusion and also results in good electrochemical behavior.

Figure 3a and b present the SEM images of LiMnPO$_4$/C and LiCo$_{0.09}$Mn$_{0.91}$PO$_4$/C composite materials, showing that the particle size varies from 50–300 nm. The particles of LiCo$_{0.09}$Mn$_{0.91}$PO$_4$/C are observed with a size between 50–200 nm with a smaller degree of agglomeration compared to LiMnPO$_4$/C. The carbon particles are seen on the surface of the active particles and are not observed with a separate
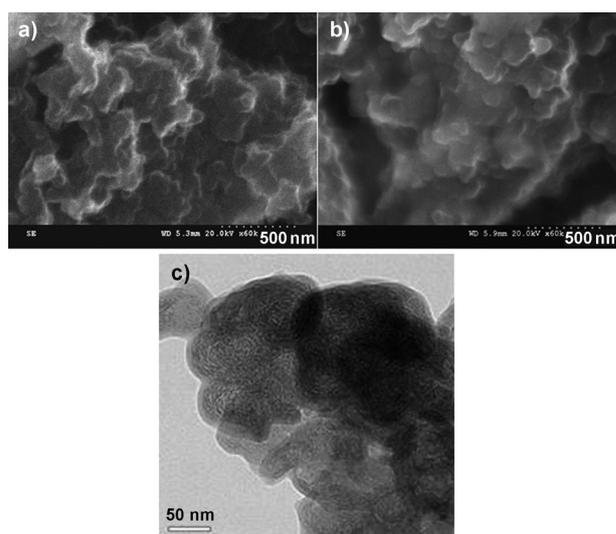

Figure 3. SEM images of a) LiMnPO$_4$/C, b) LiCo$_{0.09}$Mn$_{0.91}$PO$_4$/C, and c) TEM image of LiCo$_{0.09}$Mn$_{0.91}$PO$_4$/C composites.

morphology. Figure 3 c shows the TEM image of Li-Co$_{0.09}$Mn$_{0.91}$PO$_4$/C (30 wt%). The carbon particles are observed to be coated over the LiCo$_{0.09}$Mn$_{0.91}$PO$_4$ material. In the TEM image, particles are visible as white and black dots, the white dots are Li-Co$_{0.09}$Mn$_{0.91}$PO$_4$ materials and the black dots are carbon. The conductive carbon network decreases the particle–particle contact distance, which enhances the lithium-ion diffusion, thereby increasing the electro-chemical performance during the charge–discharge cycle.

In order to confirm the metal–ligand stretching of the synthesized materials, we carried out vibrational spectral studies, the results of which are shown in Figure 4. The factor group analysis for the olivine structures describes the Li ions occupying the 4a Whyckoff sites, which contain an inversion center. In general, vibrational motions of olivines can be classified as internal and external modes. The internal modes of olivines arise in the intramolecular vibrations of PO$_4^{3-}$ anions. The lattice vibrations or external modes originate below 400 cm^{-1}.[29] The weak bonds appeared in the range of 400–640 cm^{-1} and correspond to the bending modes (γ_3 and γ_4) involving O—P—O symmetric and antisymmetric modes and Li vibrations. Owing to the instrumental constraints, we could not record
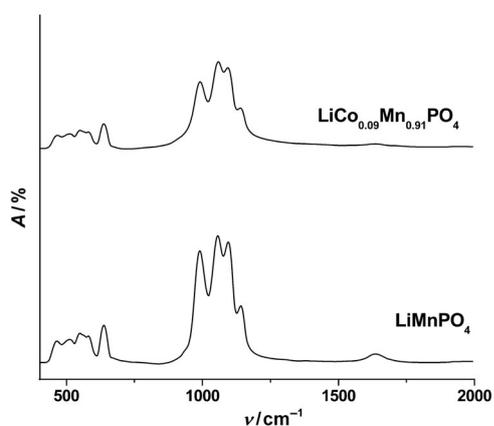

Figure 5. XPS spectra of LiCo$_{0.09}$Mn$_{0.91}$PO$_4$/C materials a) C1s, b) Li1s, c) Co2p, d) Mn2p, e) P2p, and f) O1s.

FTIR vibrations below 400 cm^{-1}. The strong bands (945–1145 cm^{-1}) appeared in the part of the spectrum which attribute the vibrations to the stretching modes of PO$_4^{3-}$ units. These bands are closely related to those of the free molecule, which correspond to the symmetric and antisymmetric P—O bonds.[30] Vibrations of both pristine and Co-doped LiMnPO$_4$ are almost similar except for the intensity of the absorbance, which indicates that a small amount of Co ions do not alter the local environment of the cations.

The oxidation state of Li, Co, Mn, P, and O of Li-Co$_{0.09}$Mn$_{0.91}$PO$_4$/C are determined through XPS measurements, as presented in Figure 5. The Li1s shows a single peak with binding energy of 53.8 eV, thus indicating that the oxidation state of Li is +1.[31] Co2p$_{3/2}$ shows a binding energy value corresponding to 782 eV, which is in close agreement with previous reports,[32] specifying that Co is present in the divalent state. Mn2p$_{3/2}$ core level shows a peak in the binding energy of 641.8 eV and confirms the oxidation state of Mn is +2.[33] The binding energies of P2p and O1s are 133.7 and 531 eV, which indicates the presence of PO$_4^{3-}$ groups.[34,35]

Figure 4. FTIR spectra of LiMnPO$_4$/C and LiCo$_{0.09}$Mn$_{0.91}$PO$_4$/C materials.

The capacity and cyclability of $LiMnPO_4$, $LiCo_{0.09}Mn_{0.91}PO_4$, and its carbon composites are determined by galvanostatic charge/discharge studies at current rates of 0.05, 0.1, and 0.2 C in the potential limit between 3–4.9 V, as shown in Figure 6 a,b. The initial discharge capacity of the pristine material (70 mAhg^{-1}) is smaller than its composite $LiMnPO_4/C$, which has a discharge capacity of 140 mAhg^{-1} at a current rate of 0.1 C. Approximately 85% of the total capacity obtained in the plateau at 4.1 V corresponds to the redox reaction of Mn^{3+}/Mn^{2+} coupled with the lithium intercalation/deintercalation into/out of the olivine structure. Similar to pristine/C composites, $LiCo_{0.09}Mn_{0.91}PO_4$ materials exhibit the discharge capacity of 148 mAhg^{-1}, whereas the

is overcome by the dopant Co^{2+} ion, which takes the site of Mn (M2 site) and displaces Mn from the Li (M1 site).[36] The high capacity delivered by carbon coated materials could be attributed to the electronic conductivity of the materials and enhanced by the conductive carbon network coated over the materials. As the individual active particles are connected by a carbon network, the active materials are fully utilized for lithium extraction and insertion reactions. Figure 6 c shows the variation of discharge capacities of $LiCo_{0.09}Mn_{0.91}PO_4/C$ at different C-rates. The discharge capacity decreases when increasing the current rate and this is attributed to the increase of electrode polarization during cycling.
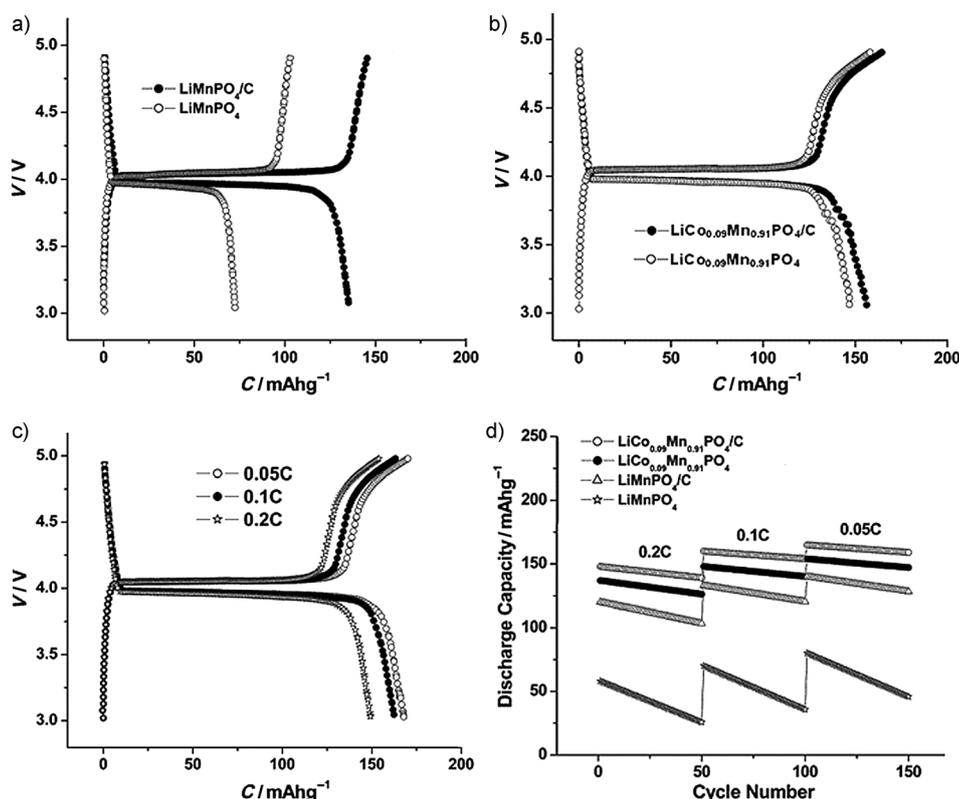

Figure 6. Charge/discharge behavior of a) $LiMnPO_4/C$, b) $LiCo_{0.09}Mn_{0.91}PO_4/C$, c) $LiCo_{0.09}Mn_{0.91}PO_4/C$ at different C-rates, and d) cycling performance at different C-rates.

Figure 6 d shows the variation of specific discharge capacity with the number of cycles of $LiMnPO_4$, $LiCo_{0.09}Mn_{0.91}PO_4$, and its carbon composites carried out at different C-rates (0.05, 0.1, and 0.2 C). Composites exhibit good cycling performance compared to its pristine and doped materials. At the end of 50th cycle, $LiMnPO_4$ and $LiCo_{0.09}Mn_{0.91}PO_4$ retain a capacity of only 50 and 94.5%, whereas the corresponding carbon composites retain 90.2% and 96.25%, respectively, at a current rate of 0.1 C. The obtained capacities and capacity retention of $LiMnPO_4$ are higher compared to previous studies.[17,18,20,21,26,37–40] The capacity fade of the $LiCo_{0.09}Mn_{0.91}PO_4/C$ composite at lower C-rate (C/20) is almost negligible, whereas 93.9% capacity retention is obtained at a current rate of 0.2 C even after 50 cycles. This excellent cycling stability of the composites has been attributed to the Co doping, which improves the dif-

$LiCo_{0.09}Mn_{0.91}PO_4/C$ composite delivers 162 mAhg^{-1} at a current rate of 0.1 C. The irreversible capacity is only 3 mAhg^{-1} and this is the lowest value reported to date at a high charge voltage (4.9 V). Martha and co-workers reported that the irreversible capacity increases when the cut-off voltage increases above 4.4 V.[25] The lowest irreversible capacity of the composites is very important in terms of usage as a rechargeable battery because the average coulombic efficiency reaches almost 99% after prolonged cycling. The poor performance of the pristine material is a result of excess Mn^{2+} occupying Li sites, and these Mn^{2+} would act as a blockage in the one dimensional transport pathway to slow down the Li ion diffusion and eventually reduce the capacity.[26] This

fusion character owing to the enlargement of the crystal lattice coupled with the carbon network that increases the electronic conductivity between the active particles. Further, the conductive carbon network reduces the lithium-ion diffusion pathway and eventually increases the charge/discharge capacity as well as the cycling stability. 10% of Co doped in $LiMnPO_4$ carbon composite provides highest discharge capacity and excellent cycling stability compared to Fe[25,41] and Mg dopants.[40] The advantage of ball milling is to control the size of the primary particles and the efficient carbon coating improves the diffusion velocity of the lithium ion. The $LiCo_{0.09}Mn_{0.91}PO_4/C$ composite materials synthesized in air atmosphere exhibit very low irreversible capacity

at high charge voltage (4.9 V) and better capacity retention compared to that of previous work.

To further understand the redox behavior of LiMnPO$_4$/C and LiCo$_{0.09}$Mn$_{0.91}$PO$_4$/C composites, the derivative curve obtained from galvanostatic charge/discharge curves are shown in Figure 7. The anodic peak and the corresponding cathodic peaks are located at 4.1 and 4 V, respectively, which is at-
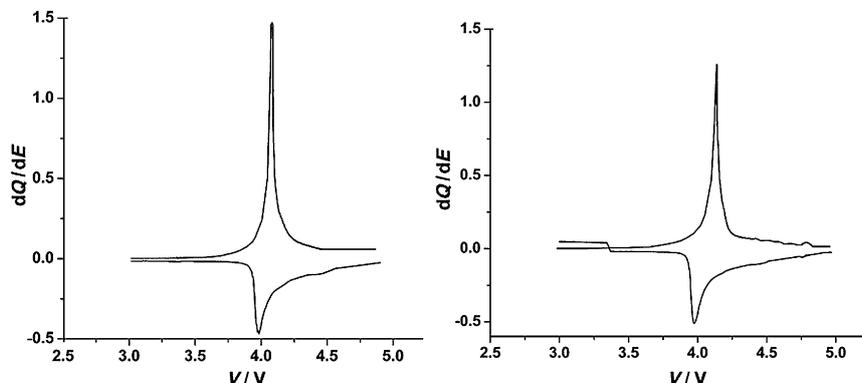
dihydrogen orthophosphate with or without Co(COOCH$_3$)$_2$·4H$_2$O were dissolved in distilled water at room temperature. This mixed solution was added to 0.1 M (7.506 g) glycine in desired proportions and then stirred to ensure that the reaction reagents were uniformly mixed. The solution was heated to 60–75 °C for 2 h, the solution then transformed into a transparent gel, and this was dried overnight at 120 °C. The resulting product was ground well and then calcined at 850 °C for 5 h in air. The calcined powders were wet (using acetone) ball milled with 30 wt % of acetylene black to obtain the composite.

TG/DTA analysis of the gel precursor was examined in an oxygen flow from 0 °C to 850 °C with a heating rate of 10 °C per minute. The calcined powders were characterized by means of XRD ('Xpert PRO PAN analytical PW 3040/60 'X'Pert PRO') using Cu$_{K\alpha}$ radiation ($\lambda = 1.5418$ A°), while the voltage and current were held at 40 kV and 20 mA ($2\theta = 10$–80°) at a scan rate of 1°/min. The surface morphology and microstructure of synthesized samples were characterized by scanning electron microscope (SEM HITACHI S-3000 H, Japan) and transmission electron microscopy (TEM, FEI-Tecnai-20 G2). FTIR spectra were recorded on a Nicolet 5DX-FTIR spectroscope by using a KBr pellet in the range of 400–2000 cm^{-1}. X-ray photoelectron spectroscopy of the synthesized powder was investigated by using VG electron spectroscopy. The powder sample was pressed into pellets and affixed to the sample holder. All spectra were recorded using an X-ray source (Al$_{K\alpha}$ radiation) with a scan range of 1200 eV binding energy. The collected high-resolution XPS spectra were analyzed using the XPS peak fitting software (XPS peak version 4.1) program. The energy scale was adjusted on the carbon peak (C1s) spectra at 284.5 eV.

The cathode was prepared by mixing 80 wt % active material, 10 wt % acetylene black, and 10 wt % polyvinylidene fluoride (PVdF) binder (for composites: 90 wt % active material and 10 wt % binder) in N-methylpyrrolidone (NMP) solvent to form a homogeneous slurry. The mixture was coated on to an aluminum foil, dried under ambient conditions, and cut into circular discs of 18 mm diameter. The cut discs were further dried under vacuum at 120 °C for 5 h. Finally, coin-type cells of the 2016 type were assembled in an argon filled glove box, in which lithium was used as the reference electrode, celgard 2400 as the separator, and LiPF$_6$ in 1:1 EC/DEC as the electrolyte. The charge–discharge cycling studies were carried out on the assembled coin cell using a programmable battery tester at different C-rates (0.05 (ca. 0.162 mAcm^{-2}), 0.1 (ca. 0.324 mAcm^{-2}), and 0.2 C (ca. 0.647 mAcm^{-2})) for 50 cycles in the potential window between 3–4.9 V.

Figure 7. Differential capacity versus potential curves of a) LiMnPO$_4$/C and b) LiCo$_{0.09}$Mn$_{0.91}$PO$_4$/C.

tributed to the redox process of Mn^{3+}/Mn^{2+} ions. This process is coupled with lithium insertion/extraction into/out of the olivine structure. The redox potential of Co^{3+}/Co^{2+} in LiCoPO$_4$ has been observed at 5.1 and 4.9 V, respectively.[12,42,43] However, in the present case, the peaks are observed in the voltage region of 4.8 and 4.7 V and could possibly be assigned to the redox couple of Co^{3+}/Co^{2+}, however, the intensity of these peaks is very small as we represent only the differential curves obtained using charge/discharge data.

Conclusions

Pristine LiMnPO4 and LiCo$_{0.09}$Mn$_{0.91}$PO$_4$ cathode materials were successfully synthesized by the sol-gel method using glycine as a chelating agent, and their corresponding composites with carbon were synthesized by the wet ball milling technique. The Co dopant increases the cell volume and this enhances the lithium-ion diffusion process. XPS studies confirm the oxidation states of Mn and Co ions to be +2. In the composites, carbon particles appeared as a coating layer over the active materials, as confirmed by TEM studies. LiMn$_{0.09}$Co$_{0.91}$PO$_4$/C nanocomposites exhibit the highest coulombic efficiency of 99 %, delivering a capacity of approximately 160 mAhg^{-1} and retains a capacity of 96.3 % over the investigated 50 cycles when cycled between 3–4.9 V at a current rate of 0.1 C.

Experimental Section

LiMnPO$_4$ and LiCo$_{0.09}$Mn$_{0.91}$PO$_4$ cathode materials were synthesized by the sol-gel method using glycine as a chelating agent. Stoichiometric amounts of Li(COOCH$_3$) 2H$_2$O, Mn(COOCH$_3$)$_2$·4H$_2$O, and ammonium

[1] B. Scrosati, J. Garche, *J. Power Sources* **2010**, *195*, 2419–2430.
[2] A. K. Padhi, K. S. Nanjundaswamy, J. B. Goodenough, *J. Electrochem. Soc.* **1997**, *144*, 1188–1194.
[3] Y. Chung, J. T. Bloking, Y. M. Chiang, *Nat. Mater.* **2002**, *1*, 123–128.
[4] S. Herle, B. Ellis, N. Coombs, L. F. Nazar, *Nat. Mater.* **2004**, *3*, 147–152.
[5] J. W. Fergus, *J. Power Sources* **2010**, *195*, 939–954.

FULL PAPERS

[6] A. Manthiram, A. Vadivel Murugan, A. Sarkar, T. Muraliganth, *Energy Environ. Sci.* **2008**, *1*, 621–638.

[7] X. Zhou, F. Wang, Y. Zhu, Z. Liu, *J. Mater. Chem.* **2011**, *21*, 3353–3358.

[8] X. Lou, Y. Zhang, *J. Mater. Chem.* **2011**, *21*, 4156–4160.

[9] S. Yang, X. Zhou, J. Zhang, Z. Liu, *J. Mater. Chem.* **2010**, *20*, 8086–8091.

[10] C. Nan, J. Lu, C. Chen, Q. Peng, Y. Li, *J. Mater. Chem.* **2011**, *21*, 9994–9996.

[11] K. F. Hsu, S. Y. Tsay, B. J. Hwang, *J. Mater. Chem.* **2004**, *14*, 2690–2695.

[12] A. Eftekhari, *J. Electrochem. Soc.* **2004**, *151*, A1456–1460.

[13] H. Fang, L. Li, Y. Yang, G. Yan, G. Li, *Chem. Commun.* **2008**, 1118–1120.

[14] C. Delacourt, L. Laffont, R. Boucher, C. Wurm, J. B. Leriche, M. Morcrette, J. M. Tarascon, C. Masquelier, *J. Electrochem. Soc.* **2005**, *152*, A913–921.

[15] A. F. Liu, Y. F. Liu, Z. H. Hu, C. C. Wang, G. Gao, Y. Y. Xu, L. Lei, *Energy Mater.* **2009**, *4*, 44–48.

[16] H. Fang, L. Li, G. Li, *Chem. Lett.* **2007**, *36*, 436–437.

[17] T. Drezen, N. Kwon, P. Bowen, I. Teerlinck, M. Isono, I. Exnar, *J. Power Sources* **2007**, *174*, 949–953.

[18] T. R. Kim, D. H. Kim, H. W. Ryu, J. H. Mo H. Moon, J. H. Lee, S. Boo, J. Kim, *J. Phys. Chem. Solids* **2007**, *68*, 1203–1206.

[19] S. K. Martha, B. Markovsky, J. Grinblat, Y. Gofer, O. Haik, E. Zinigrad, D. Aurbach, T. Drezen, G. Deghenghi, I. Exnar, *J. Electrochem. Soc.* **2009**, *156*, A541–552.

[20] R. Dominko, M. Bele, M. Gaberscek, M. Remskar, D. Hanzet, J. M. Goupil, S. Pejovnik, J. Jamnik, *J. Power Sources* **2006**, *153*, 274–280.

[21] Z. Bakenov, E. Taniguchi, *Electrochem. Commun.* **2010**, *12*, 75–78.

[22] S. M. Oh, S. W. Oh, C. S. Yoon, B. Scrosati, K. Amine, Y. K. Sun, *Adv. Funct. Mater.* **2010**, *20*, 3260–3265.

[23] U. Dettlaff-Weglikowska, N. Sato, J. Yoshida, S. Roth, *Phys. Status Solidi B* **2009**, *246*, 2482–2485.

[24] B. W. Kang, G. Cedar, *J. Electrochem. Soc.* **2010**, *157*, A808–811.

[25] S. K. Martha, J. Grinblat, O. Haik, E. Zinigrad, T. Drezen, J. H. Miners, I. Exnar, A. Kay, B. Markovsky, D. Aurbach, *Angew. Chem.* **2009**, *121*, 8711–8715; *Angew. Chem. Int. Ed.* **2009**, *48*, 8559–8563.

[26] H. Fang, Z. Pan, L. Li, Y. Yang, G. Yan, G. Li, S. Wei, *Electrochem. Commun.* **2008**, *10*, 1071–1073.

[27] S. H. Hong, A. V. Virkar, *J. Am. Ceram. Soc.* **2005**, *78*, 433–439.

[28] C. Ouyang, S. Shi, Z. Wang, X. Huang, L. Chen, *Phys. Rev. B* **2004**, *69*, 104303.

[29] T. Paquis-Ledent, P. Tarte, *Spectrochim. Acta Part A* **1974**, *30*, 673–689.

[30] C. M. Burma, R. Frech, *J. Electrochem. Soc.* **2004**, *151*, A1032–1038.

[31] X. Liu, J. Wang, J. Zhang, S. Yang, *Chin. J. Chem. Phys.* **2006**, *19*, 530–534.

[32] X. Sun, S. Wang, X. Zhang, J. Paulchen, X. Li, B. Gao, Y. Ma, *J. Colloid Interface Sci.* **2009**, *335*, 11–17.

[33] L. Yang, L. Jiao, Y. Miao, H. Yuan, *J. Solid State Electrochem.* **2010**, *14*, 1001–1005.

[34] H. Zou, G. Zhang, P. K. Shen, *Mater. Res. Bull.* **2010**, *45*, 149–152.

[35] J. Xu, G. Chen, H. Li, Z. Lv, *J. Appl. Electrochem.* **2010**, *40*, 575–580.

[36] G. X. Wang, S. L. Bewlay, K. Konstantinov, H. K. Liu, S. X. Dou, J. H. Ahn, *Electrochim. Acta* **2004**, *50*, 443–447.

[37] T. Doi, S. Yatomi, T. Kida, S. Okada, J. Yamaki, *Cryst. Growth Commun.* **2009**, *9*, 4990–4992.

[38] Y. Wang, Yifu Yang, Yanbo Yang, H. Shao, *Mater. Res. Bull.* **2009**, *44*, 2139–2142.

[39] D. Wang, H. Buqia, M. Crouzet, G. Deghenghi, T. Drezen, I. Exnar, N. H. Kwon, J. H. Miners, L. Poletto, M. Gratzel, *J. Power Sources* **2009**, *189*, 624–628.

[40] T. Shiratsuchi, S. Okada, T. Doi, J. Yamaki, *Electrochim. Acta* **2009**, *54*, 3145–3151.

[41] Y. J. Shin, J. K. Kim, G. Cheruvally, J. H. Ahn, K. W. Kim, *J. Phys. Chem. Solids* **2008**, *69*, 1253–1256.

[42] R. Ruffo, C. M. Mari, F. Morazzoni, F. Rosciano, R. Scotti, *Ionics* **2007**, *13*, 287–291.

[43] J. Wolfenstine, J. Allen, *J. Power Sources* **2004**, *136*, 150–153.